Measurement and Simulation of the Interface in a Low-Enthalpy Shock Tunnel

David R. Buttsworth*
University of Southern Queensland, Toowoomba, Queensland, 4350, Australia
Richard J. Goozée† and Peter A. Jacobs†
University of Queensland, Brisbane, Queensland, 4072, Australia

Measurements from a rake of heat flux probes installed in a 62.2 mm diameter shock tunnel have been used to deduce the thickness of the shock tube interface and its distribution across the tube for a primary shock Mach number of 2.3. The axial thickness of the interface was between about 0.32 and 0.42 m for locations from about 2.0 to 2.5 m downstream of the diaphragm station. Axisymmetric simulations using a compressible Navier Stokes solver to model the entire shock tunnel operating at this condition show a simulated interface distributed over an axial length of about 0.20 m at 2.0 m downstream of the diaphragm, thus underestimating the measured interface length by about 37 %. The simulations indicate that the diaphragm opening process has a strong influence on the interface development within the nominally inviscid core flow region of the tube. The shape of the interface in these axisymmetric simulations differs from the experimental results and this is probably because the turbulent mixing within the interface is not adequately modelled. A review of previous data on the shock tube interface development indicates that the present results (both the experimental data and numerical simulations) are consistent with interface axial lengths obtained in previous shock tube studies.

I. Introduction

SHOCK tunnels and expansion tunnels are making significant contributions to our understanding of hypersonic flow.[1] But the value of the data obtained in such facilities is a function of the precision with which the free stream flow conditions can be specified. Unfortunately, it is not possible to directly measure all of the necessary free stream flow parameters in these facilities, so some modelling is required.

In the case of reflected shock tunnels, the traditional approach for determining the free stream flow parameters uses the measurements of the initial shock tube filling conditions and the incident shock speed to calculate equilibrium reflected shock conditions. The calculated reflected shock pressure is often substantially larger than the pressure measured in the nozzle reservoir region, so an isentropic expansion from the simulated reflected shock pressure to the measured pressure is usually postulated and a new nozzle reservoir condition corresponding to the measured pressure is calculated.[2] The free stream flow parameters are then derived from the estimated nozzle reservoir conditions using a nozzle flow calculation that includes nonequilibrium chemistry when necessary. However, it is clear that if the simulated strength of the reflected shock wave is never actually achieved in practice, then the traditional approach will over-estimate the stagnation enthalpy, which consequently affects the accuracy of the derived free stream flow parameters.

More accurate estimates of the nozzle reservoir conditions may be achieved if models for shock tube losses are incorporated into the simulations. For example, various phenomenological models for momentum and energy loss mechanisms have been incorporated into quasi-one-dimensional simulations;[3] and losses associated with shock tube boundary layer development and shock interaction have also been simulated using axisymmetric Navier-Stokes solvers.[4] The fidelity of such modelling efforts is usually gauged by comparing the

*Faculty of Engineering and Surveying, University of Southern Queensland.
†Department of Mechanical Engineering, University of Queensland.

simulated shock speeds and pressure histories with experimental measurements; varying degrees of agreement have been reported. In a recent shock tunnel study using an axisymmetric solver,[5] the simulated pressure variations were more discrete than observed experimentally, and an inaccurate simulation of the shock tube interface was identified as a contributing factor.

A correct simulation of the driver gas-test gas interface is important because pressure waves generated by the interaction of the reflected shock and the interface may return to the nozzle reservoir region within the test flow period. This will be especially significant if the interface is not precisely tailored. Furthermore, the contamination of the test gas with the driver gas, which often limits the available test flow, obviously proceeds via fluid-dynamic processes associated with the interface. However, previous models of contamination in shock tubes or tunnels have generally failed to acknowledge that the spatial distribution of the interface. The leading edge of real shock tube interfaces will never be planar due to boundary layer effects, and even within the nominally inviscid core region, real shock tube interfaces may be distributed over an axial length that exceeds 10 or more tube diameters.

In an effort to evaluate and ultimately improve the numerical simulation of shock tunnel flow conditions, we have: (1) obtained new experimental data on the interface in a low-enthalpy shock tunnel; (2) applied this data to the simulation of shock tunnel operation using a quasi-one-dimensional calculation;[3] and (3) used this experimental data to evaluate the simulation of the shock tube interface using an axisymmetric scheme.[6]

For ease of experiment and simulation, we have focussed on two relatively low enthalpy conditions, the incident shock Mach numbers being 2.3 and 3.4. At these conditions the thermochemical complications normally associated with reflected shock tunnel conditions are essentially absent. However, we expect that the processes that affect the interface development at our conditions will still be operating, perhaps in some modified form, at the higher energy conditions normally produced in reflected shock tunnels.

II. Previous Interface Data

Table 1 on the following page presents previous shock tube interface data from various sources and Fig. 1 presents the majority of this data in graphical form. The initial growth of the interface length is a nonlinear function of position for certain data when $x/D < 2$, but a linear approximation seems reasonable for most results when $x/D > 2$, Fig. 1. Figure 2 summarizes the data in the form of a nondimensional growth-rate parameter $\mathrm{d}l/\mathrm{d}x$ as a function of the post-shock velocity u_2. For the each of the data sets by Glass and Patterson,[7] Ford and Glass,[8] Ikui and Matsuo,[9] and Erez et al.,[10] a single linear growth-rate corresponding to the slope of the lines illustrated in Fig. 1(a) has been plotted in Fig. 2. The remaining data in Table 1 is plotted in Fig. 2 assuming a linear growth from the diaphragm station with $l = 0$ at $x = 0$ (i.e., $\mathrm{d}l/\mathrm{d}x \approx l/x$).

The post shock velocity was chosen for the abscissa in Fig. 2 because it was postulated that higher flow speeds through the diaphragm station would generate higher mixing rates across the interface. Considering only the data by Hooker,[11] there does appear to be an increase in growth rate with increasing post shock speed (as illustrated by the broken line in Fig. 2). However, data from the other sources is not consistent with this trend, and the combined picture suggests a reasonable approximation across all conditions is $\mathrm{d}l/\mathrm{d}x \approx 0.2 \pm 0.1$. Given the large number of variables that can potentially affect the interface development and the range of conditions explored in previous studies, the level of scatter apparent in Fig. 2 is not surprising.

III. Facility, Conditions, and Instrumentation

The principal dimensions of the shock tunnel used in this work are presented in Fig. 3. The facility is located at the University of Queensland and has primarily been used for instrumentation development and pilot studies.[15–17] Two operating conditions were used as indicated in Table 2 on the next page. Interface measurements were obtained via the rake of heat flux probes illustrated in Fig. 4 with the shock tunnel operated as a shock tube (the closed-end configuration of Fig. 4 was used) at the over-tailored (nitrogen driver) condition.

The heat flux rake (Fig. 4) consisted of five stagnation heat flux gauges which were k-type surface junction thermocouples each with an outside diameter of 3mm. The construction of the surface junction thermocouples is described elsewhere,[18] and for the present work, Experiments were performed with the rake at four positions downstream of the diaphragm station: $x = 2.002$, 2.493, 2.728, and 2.945 m.

Table 1. Shock tube interface data from various sources.

Glass and Patterson,[7] Plate 1, $D = 76.2$ mm (square), driver and driven gas: air, $M_s = 1.39$, $p_1 = 40$ kPa														
l (m)	0.030	0.049	0.094											
x (m)	0.038	0.119	0.353											
Ford and Glass,[8] Plate 1, $D = 76.2$ mm (square), driver gas: He, driven gas: air, $M_s = 2.25$, $p_1 = 8.66$ kPa														
l (m)	0.131	0.183												
x (m)	0.268	0.454												
Hooker,[11] Table I, $D = 39.5$ mm, driven gas: CO_2, $x = 6.27$ m														
driver gas	He	He	Ar	He	He	H_2	H_2	He	H_2	Ar	He	He	H_2	He
p_1 (kPa)	0.0333	0.120	0.187	0.200	0.640	0.653	0.667	0.693	0.693	0.693	0.720	1.267	1.333	3.333
M_s	9.8	9.8	4.0	7.4	6.1	9.9	7.6	8.4	8.2	3.8	7.9	7.8	9.0	6.6
l (m)	2.12	1.61	1.23	1.40	1.18	1.45	1.29	1.61	1.54	1.00	1.37	1.66	1.51	1.58
Valsileva et al.,[12] Fig. 5, $D = 50$ mm, driver gas: various, driven gas: Xe														
p_1 (kPa)	5.5	5.5	5.5	1.7	1.7	1.7	13.3	13.3						
M_s	10	10	10	9	9	9	6	6						
l (m)	0.113	0.464	0.83	0.172	0.59	0.885	0.179	0.565						
x (m)	0.795	2.535	4.58	0.87	2.515	4.585	0.705	2.39						
Matsuo et al.,[9] Fig. 5, $D = 38$ mm (square), driver gas: air, driven gas: air, $x = 6.5$ m														
p_1 (kPa)	2.79	1.98	1.40	0.949										
M_s	2.4	2.5	2.6	2.8										
l (m)[a]	0.454	0.466	0.462	0.452										
Ikui and Matsuo,[13] Fig. 7, $D = 38$ mm (square), driver gas: air, driven gas: air, $x = 6.5$ m, $p_1 = 10.1$ kPa, $M_s = 1.6$[†]														
l (m)	0.027	0.041	0.051	0.055	0.059	0.061	0.064	0.070	0.072	0.072	0.076	0.083	0.084	
x (m)	0.026	0.040	0.051	0.059	0.066	0.070	0.076	0.098	0.106	0.114	0.127	0.143	0.149	
Erez et al.,[10] Fig. 6, $D = 80$ mm (square), driver gas: air, driven gas: SF_6, $p_1 = 101.3$ kPa, $M_s = 1.6$*, thick membrane														
l (m)	0.016	0.022	0.020	0.026	0.034	0.031	0.034							
x (m)	0.023	0.036	0.049	0.076	0.089	0.102	0.115							
Erez et al.,[10] Fig. 6, $D = 80$ mm (square), driver gas: air, driven gas: SF_6, $p_1 = 101.3$ kPa, $M_s = 1.6$*, thin membrane														
l (m)	0.026	0.029	0.030	0.033	0.033	0.035	0.035	0.038	0.037					
x (m)	0.063	0.064	0.072	0.081	0.089	0.098	0.106	0.115	0.123					
Present experiments, Fig. 7 (this paper), $D = 62.2$ mm, driver gas: N_2, driven gas: N_2, $p_1 = 30$ kPa, $M_s = 2.3$														
l (m)	0.318	0.421												
x (m)	2.002	2.493												
Goozée[14] simulations, Fig. 10(a) (this paper), $D = 62.2$ mm, driver gas: N_2, driven gas: N_2, $p_1 = 30$ kPa, $M_s = 2.3$														
l (m)	0.023	0.056	0.086	0.112	0.148	0.168	0.201	0.222						
x (m)	0.288	0.571	0.856	1.144	1.428	1.720	2.007	2.300						
Goozée[14] simulations, Fig. 10(b) (this paper), $D = 62.2$ mm, driver gas: He, driven gas: N_2, $p_1 = 61.4$ kPa, $M_s = 3.4$														
l (m)	0.063	0.115	0.149	0.174	0.195	0.218	0.241	0.266						
x (m)	0.268	0.545	0.834	1.130	1.430	1.731	2.036	2.341						

[a] Presented uncertainty around ± 0.09 m.

[†] Calculated from perfect gas shock relationships for given diaphragm pressure ratio, $p_{41} = 10$.

[*] Calculated from perfect gas shock relationships for given incident shock $M_s = 1.25$ in air.

Table 2. The two shock tunnel filling conditions.

Driver	Shock tube	Level of tailoring
N_2 3.25MPa	N_2 30.0 kPa	Over-tailored
He 5.60MPa	N_2 61.4 kPa	Approximately tailored

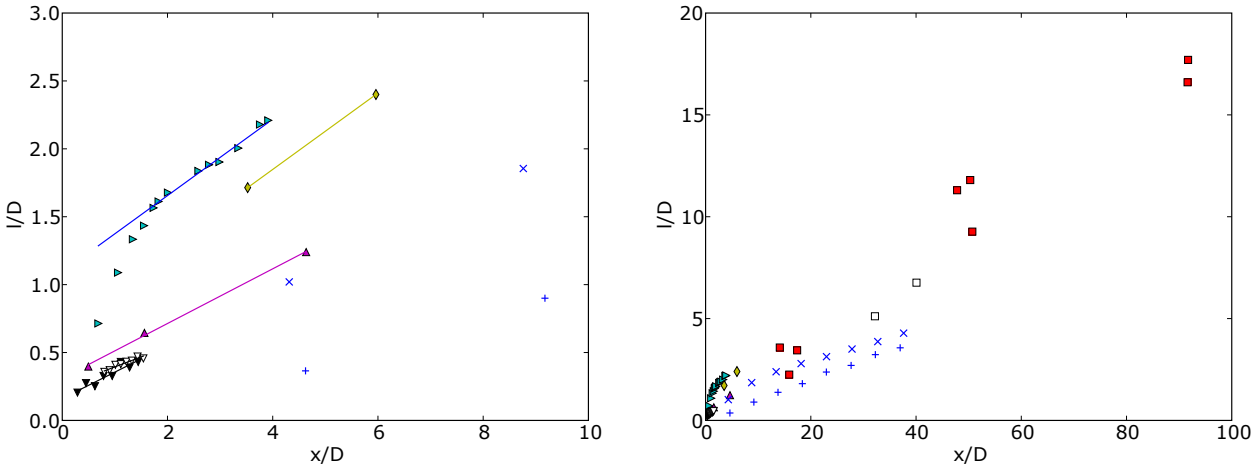

(a) Initial development showing data up to $x/D = 10$

(b) Data up to $x/D = 100$

Figure 1. Development of interface length (l/D) as it progresses along the tube (x/D).

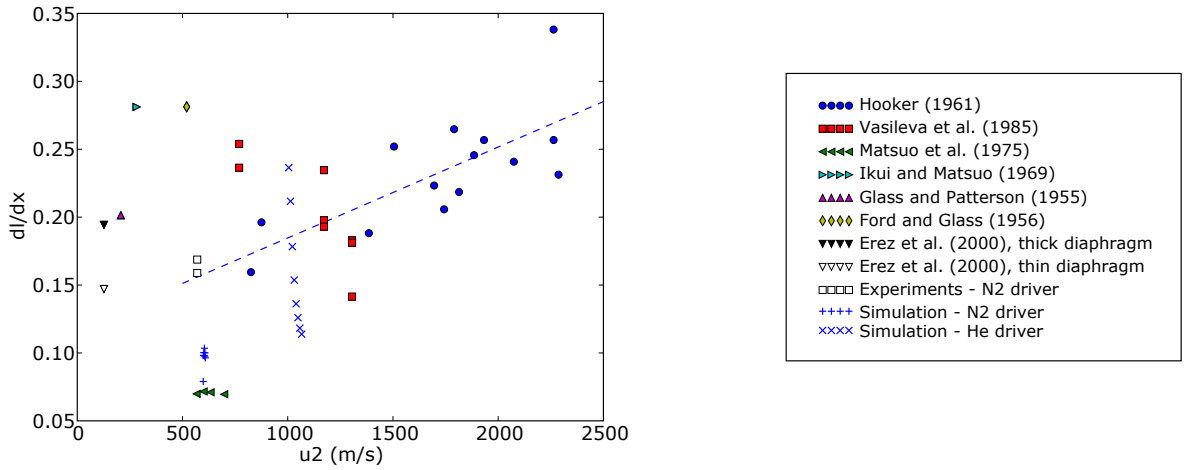

Figure 2. Rate of interface growth ($\mathrm{d}l/\mathrm{d}x$) for different post-shock speeds (u_2).

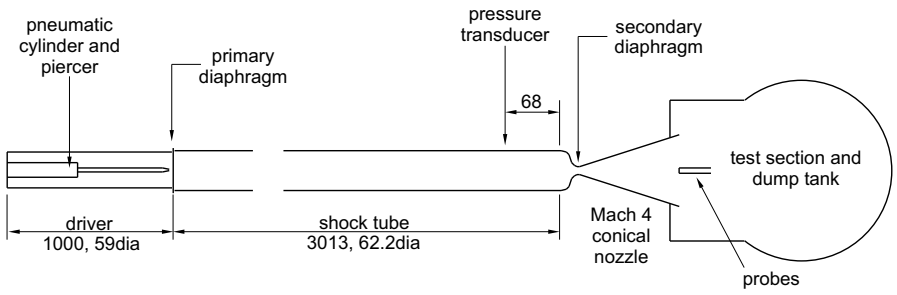

Figure 3. Illustration of the shock tunnel arrangement. Dimensions in millimetres.

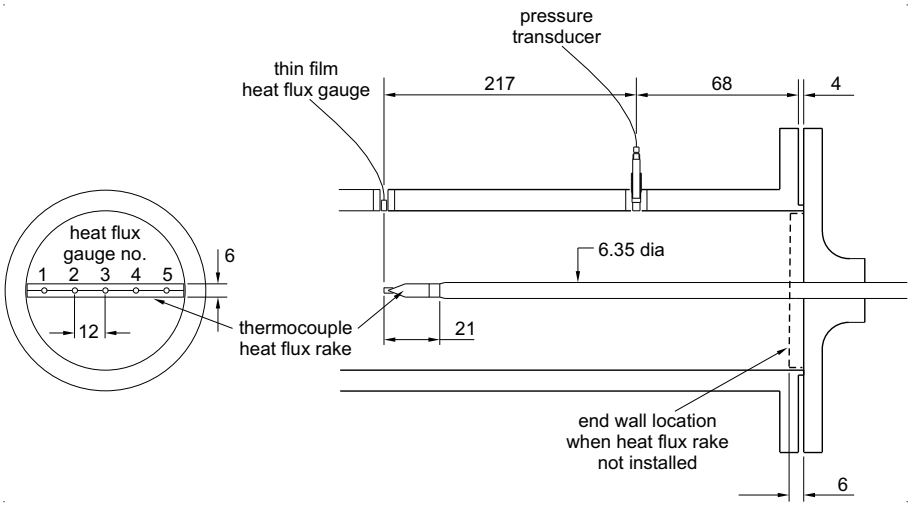

Figure 4. Illustration showing details of tube wall instrumentation and the heat flux rake with closed end of shock tube. Dimensions in millimetres.

IV. Analysis of Heat Flux Results – Interface Measurements

Sample heat flux results from probe 4 in the heat flux rake are presented in Fig. 5. The time scales in Fig. 5 are referenced to the time of incident shock arrival at the pressure transducer location. Figure 6 illustrates the method that has been adopted to define the leading and trailing edges of the interface from the heat flux signals. The rake represents a blockage to the flow behind the incident shock and when the rake was positioned at the station adjacent to the wall-mounted pressure transducer ($x = 2.945\,\mathrm{m}$) an unsteady pressure variation was registered by the transducer. Simulations of the shock tube and rake blockage effect using L1d[3] indicate that a wave system propagates upstream from the rake, but the blockage effect does not change the incident shock speed or interface trajectory significantly. The unsteady flow ahead of the rake due to its blockage effect may be responsible for the gradual increase in the heat flux signals in the post-shock flow, Fig. 5.

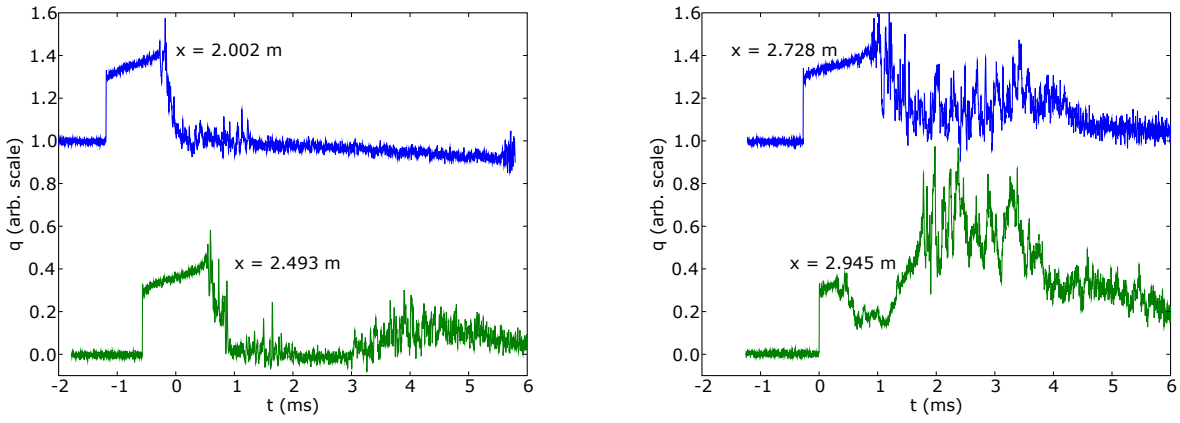

(a) Rake at $x = 2.002$ and $2.493\,\mathrm{m}$.

(b) Rake at $x = 2.728$ and $2.945\,\mathrm{m}$.

Figure 5. Sample heat flux results from gauge 4 in the rake of heat flux probes; over-tailored (nitrogen driver) condition.

Figure 7 presents the results from the analysis of the heat flux signals at the two locations closest to the diaphragm station; the interface distribution at the two downstream stations cannot be determined in

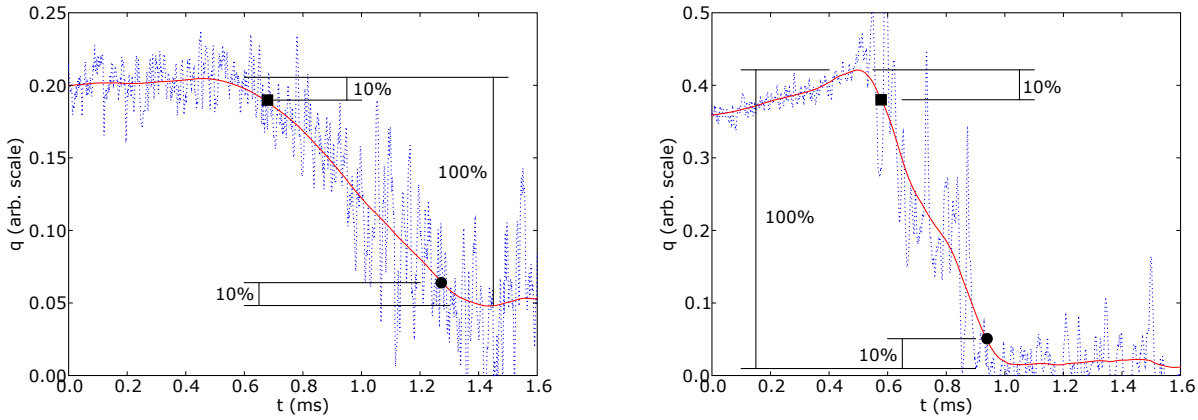

(a) gauge 1 at $x = 2.493\,\mathrm{m}$.

(b) gauge 4 at $x = 2.493\,\mathrm{m}$.

Figure 6. Illustration of the interface definition based on heat flux signals: interface leading edges indicated by the squares and trailing edges indicated by the circles.

the manner described above because the reflected shock arrives at these stations ($x = 2.728$ and $2.945\,\mathrm{m}$) at about the same time or earlier than the interface. Based on the three heat flux gauges closest to the centre line of the tube (gauges 3, 4, and 5), time lag between the arrival of the interface leading edge and trailing edges is around $0.37\,\mathrm{ms}$ for both of the heat flux rake locations presented in Fig. 7. Axisymmetric simulations (Section V) indicate the centre of the interface is probably traveling at about $570\,\mathrm{m/s}$ in this case, so the axial length of the interface is around $0.21\,\mathrm{m}$ near the tube centreline. However, gauges 1 and 5 (the gauges nearest the tube wall) indicate that the arrival of the trailing edge of the interface is delayed relative to its arrival at the other gauges. The overall length of the interface reported in Table 1 was obtained by taking the difference between the average leading edge arrival time at gauges 2, 3, and 4 and the average trailing edge arrival time at gauges 1 and 5 (and by again assuming the centre of the interface was travelling at $570\,\mathrm{m/s}$).

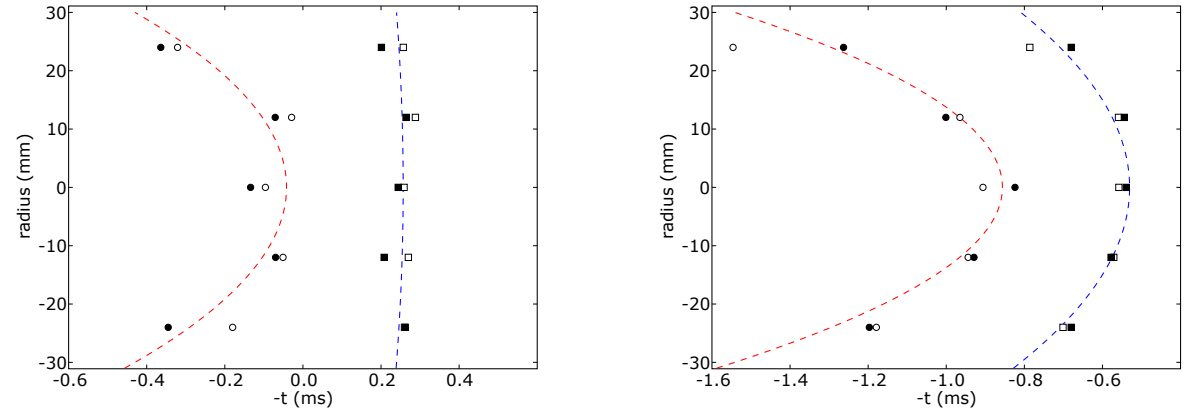

(a) Rake at $x = 2.002\,\mathrm{m}$.

(b) Rake at $x = 2.493\,\mathrm{m}$.

Figure 7. Arrival times of the leading edges (squares) and trailing edges (circles) of the interface relative to the time of incident shock arrival at the pressure transducer location. Two data sets are presented (represented by the open and filled symbols) resulting from a repeated run at nominally identical conditions for the two locations.

V. Interface Simulations

A. Quasi-One-Dimensional Simulations

To illustrate the sort of improvements that might be achieved by correctly simulating the interface, consider Fig. 8 which compares quasi-one-dimensional simulations of the shock tube pressure using L1d[3] with pressure measurements at the station indicated in Figs. 3 and 4 in the over-tailored (nitrogen driver) condition. For this experiment, the shock tunnel was operated as a shock tube with a closed end, but the heat flux rake was not present, Fig. 4. L1d provides a Lagrangian simulation of the gas dynamics within the facility and accommodates area changes between sections of the tube, but normally the interface between adjacent cells remains discrete – no mixing takes place between adjacent cells. The "simulation" result in Fig. 8 illustrates the discrete wave effects associated with the reflected shock interacting the with driver gas-test gas interface. In the "interface simulation" result in Fig. 8, the properties of the cells in the vicinity of the driver gas-test gas interface were adjusted according to an assumed linear density distribution over an axial length of around 300 mm (close to the value measured at $x = 2.002$ m), Table 1.

Clearly the compression process associated with the over-tailoring of this condition (the pressure rise from about 1.2 ms onwards on the scales in Fig. 8) is simulated with high fidelity when the distributed interface simulation is employed. The observed agreement between the simulated and the experimental pressure measurements has been achieved because of prior knowledge of the interface thickness at this particular operating condition. If the only source of information on interface lengths is an empirical data base such as Table 1, then the specified interface length might be in error by 50 % or more at other operating conditions. Thus it is appropriate to seek a shock tunnel simulation that incorporates a model for the interface but does not rely on existing interface length measurements. Axisymmetric simulations can be used to model the interface without relying directly on existing experimental data for interface lengths, as demonstrated in the next section.

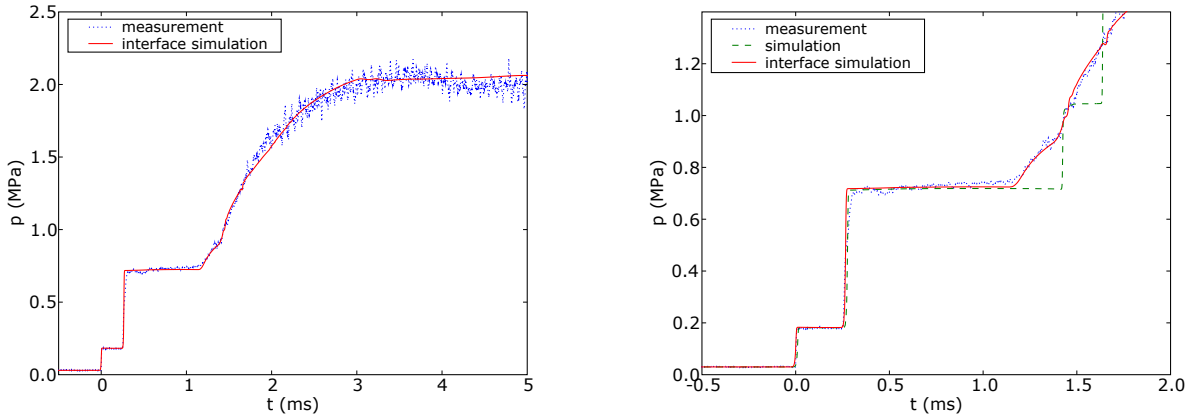

Figure 8. Comparison of L1d simulations and experimental pressures at the pressure transducer station $x = 2.945$ m.

B. Axisymmetric Simulations

The modelling of the diaphragm opening process in the axisymmetric simulations, is a major contributor to the resulting axial length of the interface. This is demonstrated by considering the simulated interface shapes for instantaneous diaphragm removal Fig. 9, and comparing these with the simulated interfaces obtained using the iris model[14] for diaphragm rupture, Fig. 10. In the case of the case of the over-tailored condition (which uses the nitrogen driver), an instantaneous removal of the diaphragm results in an almost planar contact region apart from the boundary layer effects near the tube wall (Fig. 9(a)). The interface accelerates from rest to about 600 m/s within about 3 tube diameters downstream of the diaphragm station, Fig. 11(a), and then a marginal increase in speed perhaps occurs (as suggested by the regression in Fig. 11(a)) until the interface interacts with the reflected shock (not shown). Throughout the interface acceleration process, the

driver gas retains a higher density than the driven gas, and hence the interface ought to be stable according to the Rayleigh-Taylor stability criterion, and certainly the simulated shape for the instantaneous diaphragm removal supports this notion, Fig. 9(a).

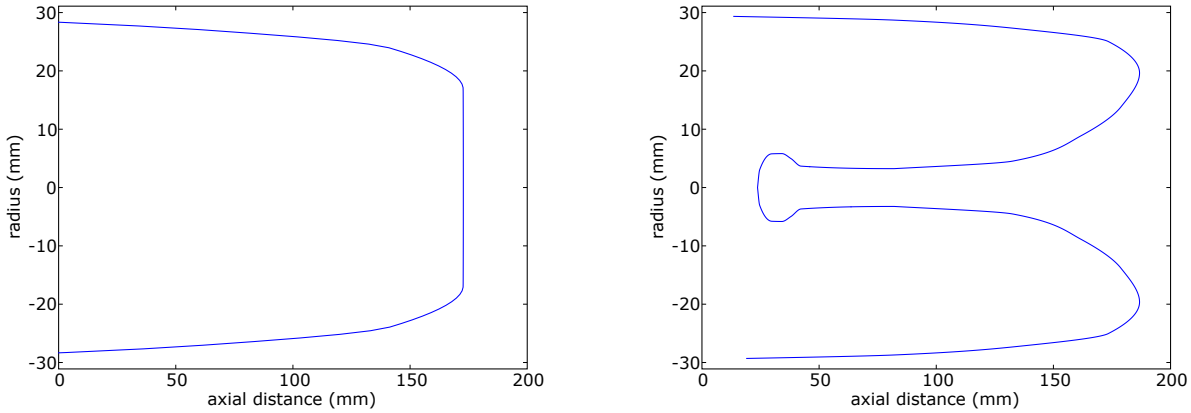

(a) Over-tailored condition, nitrogen driver.

(b) Approximately-tailored condition, helium driver.

Figure 9. Simulated interface shapes for instantaneous diaphragm removal.

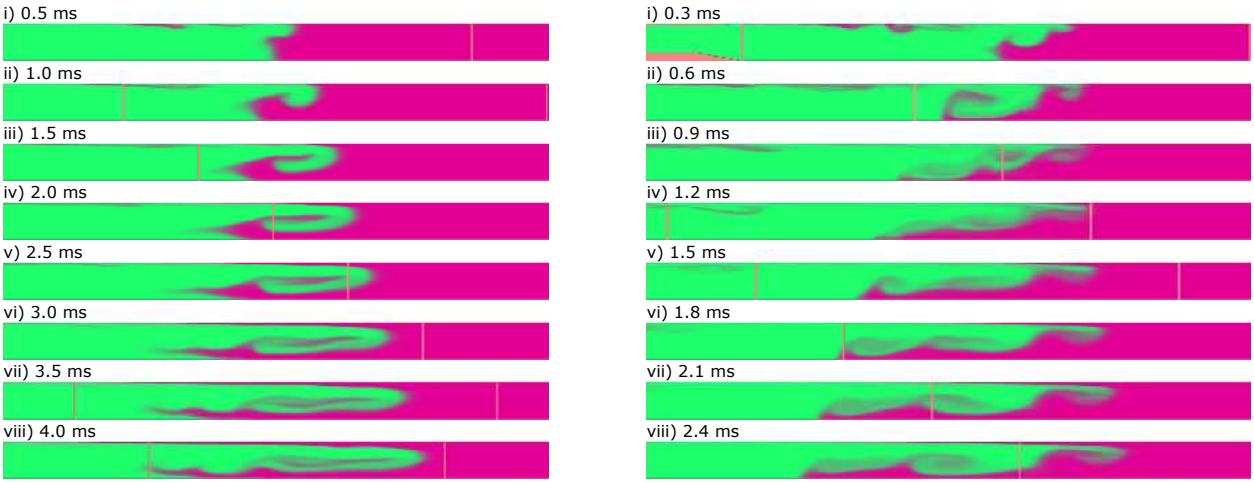

(a) Over-tailored condition, nitrogen driver.

(b) Approximately-tailored condition, helium driver.

Figure 10. Simulations of the interface development at various times relative to initiation of diaphragm rupture. Flow from left to right; iris diaphragm opening model used; times relative to initiation of diaphragm rupture; each frame displays a region of the tube from the centreline (lower horizontal edge) to its radius (upper horizontal edge).

In contrast, simulations of the over-tailored condition with the iris model for the diaphragm rupture produce an annular tongue of driver gas that penetrates the driven gas as illustrated in Fig. 10(a). (With the iris model, the open area of the diaphragm is assumed to increase as a linear function of time, with the overall time for the process being estimated from the experimental data.[14,19]) There are at least two possible effects that potentially contribute to the interface distortion observed in the over-tailored case with the iris model for diaphragm opening. Firstly, when the finite diaphragm opening time is simulated with the iris model, a radial shock wave emerges from the diaphragm station ahead of the interface and reflects off the wall of the shock tube, creating a sequence of transverse waves. These transverse waves process the interface as it emerges from the diaphragm station and in the process, vorticity is generated at the interface

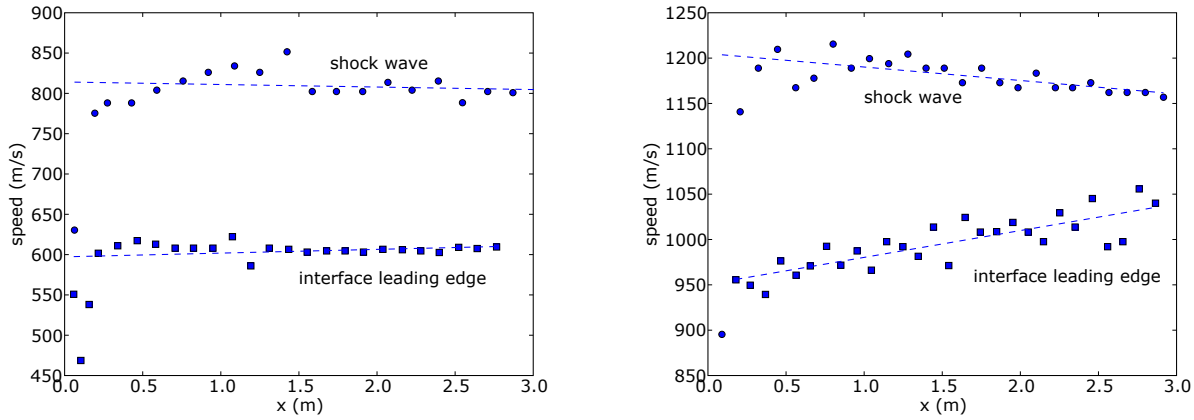

(a) Over-tailored condition, nitrogen driver.

(b) Approximately-tailored condition, helium driver.

Figure 11. Simulated shock speeds and interface leading edge speeds.

due to the interaction of the pressure gradient across the shock waves and the density gradient across the interface. The vorticity deposited at the interface during the diaphragm opening process could contribute to subsequent development (distortion) of the interface as it travels down the tube. Secondly, during the simulated diaphragm rupture, a Mach disk is established downstream of the diaphragm station causing lower speeds in the driver gas on the centre line of the shock tube. With the development of the boundary layer on the shock tube, the driver gas flow speed reaches a peak between the tube centre line and the wall, thus contributing to the development of an annular tongue of driver gas that penetrates the driven gas as illustrated in Fig. 10.

In the case of the helium driver condition, the interface appears unstable even in the instantaneous diaphragm removal simulation, Fig. 9(b). This is probably because the condition is actually slightly undertailored – the density in the expanded driver gas is lower than that of the shock compressed driven gas by about 10 %, and the interface accelerates as it travels down the tube, Fig. 11(b). However, with the introduction of the iris diaphragm model, further distortion of the interface occurs (Fig. 10(b)) presumably because of similar mechanisms that operate in the over-tailored (nitrogen driver) condition. The axial length of the interface (apart from the boundary layer on the shock tube wall) increases by a factor of about 1.6 with the introduction of the iris model for diaphragm opening.

The simulated interface shape for the nitrogen driver (over-tailored) condition in Fig. 10(a) is very different to the experimentally-determined interface shape, Fig. 7. For example, in the simulations, the driver gas penetrates the driven gas as an annular tongue and the driver gas will therefore first appear at any given downstream station at an off-axis location. In the experiments however, at both stations downstream of the diaphragm, the driver gas first appears on the tube axis. For the simulations, diffusion across the interface was via laminar and numerical mechanisms only and we expect this is the main reason that the experimental interface shape is not simulated accurately.

The axial length of the simulated interfaces has been identified from each of the frames in Fig. 10 by taking the difference between the furthermost downstream position of the driver gas and the furthermost upstream position of the driven gas (apart from the boundary layer). This development of the simulated interfaces is reported in Table 1 and Figs. 1 and 2. In the case of the nitrogen driver (over-tailored) condition, the axisymmetric simulations underestimate the axial length of the interface relative to the experimental results by about 37 %. In the case of the helium driver (approximately-tailored) condition, the axisymmetric simulations indicate an axial growth rate that decreases from about 0.24 to 0.11 (Fig. 2) over the period presented in Fig. 10(b). Interestingly, the simulated interface lengths and growth rates for both conditions lie within the scatter reported in the combined experimental results, Fig. 2.

VI. Conclusion

A wide range of interface growth rates have been observed in prior shock tube studies, but the overall picture suggests $\mathrm{d}l/\mathrm{d}x \approx 0.2 \pm 0.1$. New measurements of the interface thickness and its radial distribution have been obtained in a shock tunnel using a rake of heat flux probes at an over-tailored condition with an incident shock Mach number of 2.3. Assuming a linear growth in the interface length downstream of the diaphragm, our measurements indicate a growth rate $\mathrm{d}l/\mathrm{d}x \approx 0.16$, which is consistent with earlier results.

Quasi-one-dimensional gas-dynamics simulations using a distributed interface based on these experimental measurements accurately capture the pressure rise associated with the over-tailoring of this condition. However, such improvements in simulation may not be achieved in other shock tunnels and conditions unless the interface length is known or can be estimated with sufficient accuracy from the existing data.

We have also performed axisymmetric simulations in an attempt to progress our interface modelling beyond the empirical approach of the quasi-one-dimensional simulations. Axisymmetric Navier Stokes simulations underestimate the axial length of the interface in the over-tailored condition by about 37 %. In these simulations it was necessary to implement an iris model for the diaphragm opening process, with the overall time for opening being estimated using previous experimental data. Axisymmetric simulations were also performed for an approximately-tailored condition, though we do not have any direct measurements of the interface at this condition. The diaphragm opening process has a strong influence on the simulated interface length in both the over-tailored and approximately-tailored conditions.

The axisymmetric simulations have not reproduced the correct the interface shape. In the axisymmetric simulations, diffusion across the interface was via laminar and numerical mechanisms only and we expect this, together with the non-three-dimensional opening of the iris model, is the main reason the experimental interface shape is not simulated accurately. The present interface measurements and simulations are consistent with data derived from other sources, but improvements in the axisymmetric simulations should be possible by introducing a model for turbulent diffusion across the interface.

Acknowledgement Computer time for the simulations was supported by the High Performance Computing unit at the University of Queensland.

References

[1] *Advanced hypersonic test facilities*, edited by F. Lu and D. Marren, AIAA, 2002.

[2] Jacobs, P. A. and Gardner, A. D., "Gas-dynamic Modelling of the HEG Shock Tunnel," Tech. rep., Institute for Aerodynamics and Flow Technology German Aerospace Center, Goettingen, Jan. 2003.

[3] Jacobs, P. A., "Quasi-one-dimensional Modelling of a Free-Piston Shock Tunnel," *AIAA Journal*, Vol. 32, No. 1, 1994, pp. 137–145.

[4] Sharma, S. P. and Wilson, G. J., "Computations of axisymmetric flows in hypersonic shock tubes," *Journal of Thermophysics and Heat Transfer*, Vol. 10, No. 1, 1996, pp. 169–176.

[5] Goozée, R. J., Jacobs, P. A., and Buttsworth, D. R., "Simulation of a complete reflected shock tunnel showing a vortex mechanism for flow contamination," *Shock Waves*, Vol. 15, No. 3-4, 2006, pp. 165–176.

[6] Jacobs, P. A., "MB_CNS: A computer program for the simulation of transient compressible flows," Report 10/96, Department of Mechanical Engineering, The University of Queensland, Dec. 1996.

[7] Glass, I. I. and Patterson, G. N., "A Theoretical and Experimental Study of Shock-Tube Flows," *Journal of the Aeronautical Sciences*, Vol. 22, No. 2, 1955, pp. 73–100.

[8] Ford, C. A. and Glass, I. I., "An Experimental Study of One-Dimensional Shock Wave Refraction," *Journal of the Aeronautical Sciences*, Vol. 23, No. 2, 1956, pp. 189–191.

[9] Matsuo, K., Kage, K., and Kawagoe, S., "The Interaction of a Reflected Shock Wave with the Contact Region in a Shock Tube," *Bulletin of the JSME*, Vol. 18, No. 121, 1975, pp. 681–688.

[10] Erez, L., Sadot, O., Oron, D., Erez, G., Levin, L. A., Shvarts, D., and Ben-Dor, G., "Study of the Membrane Effect on Turbulent Mixing Measurements in Shock Tubes," *Shock Waves*, Vol. 10, 2000.

[11] Hooker, W. J., "Testing Time and Contact-Zone Phenomena in Shock-Tube Flows," *Physics of Fluids*, Vol. 4, No. 12, 1961, pp. 1451–1463.

[12] Vasileva, R. V., Zuev, A. D., Moshkov, V. L., Tkhorik, L. G., and Shingarkina, V. A., "Turbulent Mixing of Driver and Driven Gases in a Shock Tube Channel," *Journal of Applied Mechanics and Technical Physics*, Vol. 26, No. 2, 1985, pp. 271–277.

[13] Ikui, T. and Matsuo, K., "Investigations of the Aerodynamic Characteristics of the Shock Tubes (Part 1, The Effects of Tube Diameter on the Tube Performance," *Bulletin of the JSME*, Vol. 12, No. 52, 1969, pp. 774–782.

[14] Goozée, R. J., *Simulation of a complete shock tunnel using parallel computer codes*, Ph.D. thesis, University of Queensland, Australia, 2003.

[15]Austin, J. M., Jacobs, P. A., Kong, M. C., Barker, P., Gammie, R., and Littleton, B. N., "The Small Shock Tunnel Facility at UQ," Report 2/97, Department of Mechanical Engineering, The University of Queensland, July 1997.

[16]Buttsworth, D. R. and Jacobs, P. A., "Total temperature measurements in a shock tunnel facility," *Proceedings of the 13th Australasian Fluid Mechanics Conference*, edited by M. C. Thompson and K. Hourigan, Vol. 1, Department of Mechanical Engineering, Monash University, Melbourne, Australia, Dec. 1998, pp. 51–54.

[17]Craddock, C. S., *Computational optimization of scramjets and shock tunnel nozzles*, Ph.D. thesis, University of Queensland, Australia, 1999.

[18]Buttsworth, D. R., "Assessment of effective thermal product of surface junction thermocouples on millisecond and microsecond time scales," *Experimental Thermal and Fluid Sciences*, Vol. 25, No. 6, 2001, pp. 409–420.

[19]Rothkopf, E. M. and Low, W., "Diaphragm Opening Process in Shock Tubes," *Physics of Fluids*, Vol. 17, No. 6, 1974, pp. 1169–1173.